GSI

Preprint 2003 - 10
April

# Searching for the $^{5}$H resonance in the t + n + n system

M. Meister, L.V. Chulkov, H. Simon, T. Aumann, M.J.G. Borge, Th. W. Elze, H. Emling, H. Geissel, M. Hellström, B. Jonson, J. V. Kratz, R. Kulessa, Y. Leifels, K. Markenroth, G. Münzenberg, F. Nickel, T. Nilsson, G. Nyman, V. Pribora, A. Richter, K. Riisager, C. Scheidenberger, G. Schrieder, O. Tengblad

Gesellschaft für Schwerionenforschung mbH
Planckstraße 1 • D-64291 Darmstadt • Germany
Postfach 11 05 52 • D-64220 Darmstadt • Germany

# Searching for the $^5$H resonance in the t + n + n system

M. Meister [a,b], L.V. Chulkov [b,c], H. Simon [d], T. Aumann [b,e], M.J.G. Borge [f], Th. W. Elze [g], H. Emling [b], H. Geissel [b], M Hellström [b], B. Jonson [a], J. V. Kratz [e], R. Kulessa [h], Y. Leifels [b], K. Markenroth [a], G. Münzenberg [b], F. Nickel [b], T. Nilsson [i], G. Nyman [a], V. Pribora [c], A. Richter [d], K. Riisager [j], C. Scheidenberger [b], G. Schrieder [d] and O. Tengblad [f]

[a] *Experimentell Fysik, Chalmers Tekniska Högskola and Göteborgs Universitet, S–412 96 Göteborg, Sweden*

[b] *Gesellschaft für Schwerionenforschung (GSI), Planckstr. 1, D–64291 Darmstadt, Germany*

[c] *Kurchatov Institute, RU–123182 Moscow, Russia*

[d] *Institut für Kernphysik, Technische Universität, D–64289 Darmstadt, Germany*

[e] *Institut für Kernchemie Johannes Gutenberg-Universität, D–55099 Mainz, Germany*

[f] *Instituto Estructura de la Materia, CSIC, E–28006 Madrid, Spain*

[g] *Institut für Kernphysik Johann-Wolfgang-Goethe-Universität, D–60486 Frankfurt, Germany*

[h] *Instytut Fizyki, Universytet Jagielloński, PL–30-059 Kraków, Poland*

[i] *EP-Division, CERN, CH–1211 Genève 23 , Schweiz*

[j] *Institut for Fysik og Astronomi, Aarhus Universitet, K–8000 Aarhus C, Denmark*

*Preprint submitted to Elsevier Preprint* *4 February 2003*

**Abstract**

The unbound hydrogen isotopes $^{4,5}$H have been studied in the one-proton knock-out channel of $^{6}$He (240 MeV/u) impinging on a carbon target. The triton fragments originating from this channel were detected in coincidence with neutrons. Relative energy spectra as well as energy and angular correlations have been studied for the $t$+$n$ and $t$+$n$+$n$ systems. The analysis of the energy and angular correlations by the method of hyperspherical harmonic expansion allows to determine the relative weights of the most relevant partial waves in the three-body $t$+$n$+$n$ final state. It is shown that the neutrons to a large extent occupy the $p$-shell and that the $I^{\pi} = 1/2^{+}$ state is strongly populated as expected for the $^{5}$H ground state. No evidence for a narrow resonance in the $t$+$n$+$n$ system is obtained, instead a broad structure peaked at 3 MeV above the threshold with about 6 MeV as a full width at half maximum is observed. The two-body $t$+$n$ system reveals a resonance compatible with earlier results for $^{4}$H.

*Key words:* PACS number(s): 27.10+h, 25.60.Gc

## 1 Introduction

Experimental studies of heavy hydrogen isotopes (4≤A≤7) have recently attracted much interest and some intriguing results have been reported. The structure of a heavy hydrogen nucleus is expected to be similar to that of neutron-rich helium isotopes, namely, an inert core surrounded by valence neutrons [1–3]. The $^{5}$H isotope, with an even neutron number, could be less unbound than $^{6}$H or even $^{4}$H due to the neutron pairing energy. However, the width of this state, estimated in a conventional R-matrix approach is extremely large (10-15 MeV) due to the absence of Coulomb and centrifugal barriers in the $t$+ di-neutron channel [1,2]. For the isotopes with odd neutron number ($^{4}$H and $^{6}$H), the experimental studies revealed their ground states as comparatively narrow resonances at 2-3 MeV above the dissociation threshold [1,4]. The experiments aiming at an identification of $^{5}$H have, however, given contradictory results [4–7]. Several attempts to find this resonance in different types of nuclear reactions have been unsuccessful. Evidence for $^{5}$H as a broad state at 5.2(4) MeV was obtained in the $^{7}$Li($^{6}$Li,$^{8}$B) reaction [8]. A recent experiment reports the ground state at 5(1) MeV with a width of 3 MeV in $^{9}$Be($\pi^{-}$,pt) and $^{9}$Be($\pi^{-}$,dd) reactions [5]. However, a peak in a spectrum of protons from the $^{3}$H(t,p) reaction, consistent with a $^{5}$H state at 1.8 MeV, was found in Ref. [9]. The observation of the $^{5}$H ground state at 1.7(3) MeV with the width 1.9(4) in the $^{6}$He(p,2p) reaction was reported [6] about a year ago. The most recent experiment, again using the $^{3}$H(t,p) reaction revealed a peak in the experimental spectra of protons consistent with a $^{5}$H resonance at the

same energy as in Ref. [6] but with a width less than 500 keV [7].

The main experimental method for the identification of the unbound H isotopes in the experiments mentioned above is the missing-mass method combined with an analysis based on deviations of the measured spectra from phase space evaluations. However, this method should be used with caution at low energies when many particles are present in the final state, since the phase space may be modified by different types of inter-particle interactions or excitations of intermediate fragments and their subsequent decays. There are many cases where the reaction mechanism might mimic a resonance in the experimental spectrum, see e.g. Ref. [10]. At very high energies, the reaction mechanism is much simpler than at low energies. The nucleon knockout channel dominates, and by a selection of a structurally close projectile, resonances observed by means of a relative energy measurement are almost free from background due to other reaction mechanisms [11,12].

The $t$+$n$+$n$ data presented in this paper were obtained in proton knockout reactions from a 240 MeV/u $^{6}$He beam in a carbon target. Nucleon knockout is the dominant reaction mechanism at this energy, and Glauber type models are well suited to describe the data. The $^{6}$He structure is predominantly an inert $\alpha$-core with two valence neutrons in the $p_{3/2}$-shell with their momenta coupled to zero [13]. A sudden knockout of a proton from the alpha particle will result in a system with a triton and two valence neutrons in the same configuration as they had in the projectile. Thus the most likely ground-state configuration of $^{5}$H, i.e. a triton coupled with two $p_{3/2}$ neutrons to spin $I^{\pi}=1/2^{+}$ is already preformed. The $^{4}$H resonance with a triton core and one neutron in the $p_{3/2}$-shell was also investigated from the same data by selecting events where one of the two neutrons fell outside the detector acceptance of the set-up. This means that it is well separated in momentum space from the detected neutron and triton and that the residual interaction between the two neutrons is suppressed. The present result on $^{4}$H was used as a check of the assumed reaction mechanism by comparing with previously published data from the extensively studied $^{4}$H [4].

The paper is structured as follows: Section 2 provides experimental details about the essential steps during data analysis. In section 3, the properties of $^{4}$H are studied in the $t$+$n$ relative energy spectrum. Furthermore, the experimental $t$+$n$+$n$ relative energy spectrum is shown and compared with microscopic dynamical calculations in a three body continuum. Section 4 is devoted to a detailed analysis of different types of correlations within the three-body system. The influence of the $t$-$n$ and $n$-$n$ final state interaction on the $t$+$n$+$n$ relative energy spectrum is analysed using an event-mixing procedure. In addition, the experimental energy and angular correlations are analysed using a restricted set of hyperspherical harmonics (HH), in order to obtain the relative weights of the predominant partial waves and assign the spin and parity to

the broad structure seen in the $t$+$n$+$n$ relative energy spectrum. Finally, the resemblance between the structure of $^{5}$H, $^{6}$He and $^{6}$Be is discussed.

## 2 Experimental method and analysis procedure

The radioactive beam of 240 MeV/u $^{6}$He was produced in a 8 g/cm$^{2}$ Be production target by fragmentation of a primary $^{18}$O (340 MeV/u) beam from the heavy-ion synchrotron SIS at GSI, and subsequently separated in the fragment separator FRS by magnetic analysis. The beam was then directed towards a carbon target (thickness 1.87 g/cm$^{2}$) placed directly in front of the large-gap dipole magnetic spectrometer, ALADIN. The experimental setup is described in detail in Ref. [14], here the main features relevant for the analysis presented in this paper are summarized.

In the present experiment only events containing a charged triton fragment and neutrons were chosen for the analysis. The tritons produced in the $^{6}$He fragmentation reaction were deflected and analyzed by the dipole magnet ALADIN in conjunction with position-sensitive multi-wire drift chambers and a plastic time-of-flight wall. The neutrons, recorded in coincidence with the tritons, were detected in the large area neutron detector LAND, covering about $\pm$80 mrad around the beam direction. The momentum vectors of the triton and the neutrons were determined for each separate event. The momentum distributions of the tritons, neutrons and the reconstructed $^{5}$H reveal a peak centered at projectile velocity in longitudinal direction. The measured momenta were transformed to the projectile rest frame by using relativistic expressions. In this system the longitudinal and transverse widths of the momentum distributions are the same.

The experimentally determined probability of detecting two neutrons together with one triton in coincidence is three times larger than the probability to observe two neutrons in coincidence with a $^{4}$He [14] [1]. These facts give evidence for a dominant contribution of the proton knockout process, which leads to a final state of $t$+$n$+$n$, where the fragments are expected to be close in momentum space. The knockout mechanism of a tightly bound proton is similar to that of a loosely bound neutron, which was discussed in Ref. [16] describing an experiment using $^{11}$Be and $^{11}$Li beams to study the properties of $^{10}$Li.

The overall experimental resolution with regard to decay energies for the studied reaction channels was obtained from Monte-Carlo simulations, calculated applying the measured detector responses. The general trend in both the two-

[1] Fragmentation of $^{6}$He into $^{4}$He and neutrons is dominated by the one-neutron knockout channel and the knockout neutrons are strongly deflected [15].

body and three-body system is the same, where at low decay energy the resolution is about 150 keV and increases to 800 keV at 8 MeV. The Monte-Carlo simulations also give the detection efficiency. In the two-neutron case at low energy a decrease in efficiency due to the limited resolving power for two neutrons at small relative distances in LAND is observed. Further, due to the finite solid angle of the neutron detector the efficiency also decreases at higher energies. All the measured distributions have been corrected for efficiency which includes distortions introduced by the tracking routine and restricted acceptance of the experimental setup. For a detailed discussion see Refs. [14,17].

The background was measured without target and contributes 35% in the $t$+$n$ relative energy spectrum, and 10% in the $t$+$n$+$n$ relative energy spectrum. The efficiency to detect 240 MeV neutrons in LAND is 80% [18], which means that there is a 20% probability that one of the two neutrons will not be detected in the two-neutron case and might therefore be misinterpretated as a one-neutron event. Simulations showed that these misidentified one-neutron events contribute to 10% in the $t$+$n$ relative energy spectrum. Further, the simulations also showed that 5% of one-neutron events are misinterpretated by the tracking algorithm to be two-neutron events, which give a contribution in the order of 20% in the $t$+$n$+$n$ relative energy spectrum. The measured spectra were corrected for these types of background by subtracting corresponding simulated spectra.

## 3 Relative energy spectra

The invariant mass method is a widely used tool searching for resonance states. The relative energy spectra differ from the invariant mass spectra only in the energy scale by the subtracted masses of the involved fragments. This chapter will be devoted to the reconstructed relative energy spectra from the measured relative momenta of triton and neutron(s), in the two systems $t$+$n$ and $t$+$n$+$n$.

### *3.1 The $^4H$ case*

First, we look at the relative energy spectra in the $t+n$ system. The $^4$H result presented here was obtained from events where one of the two neutrons does not fall into the LAND acceptance. Here, the selection of the events was made in order to reduce the interaction effects with the second neutron, and the undetected neutron is well separated in momentum space from the detected neutron and triton. The $t$+$n$ energy spectrum from events where both neutrons are detected is discussed in detail in Appendix A.

The triton - neutron relative momentum is given as:

$$\mathbf{p}_{tn} = \frac{m_t m_n}{m_t + m_n}\left(\frac{\mathbf{p}_t}{m_t} - \frac{\mathbf{p}_n}{m_n}\right) \tag{1}$$

Here, the triton($\mathbf{p}_t$) and neutron ($\mathbf{p}_n$) momenta are defined in the projectile rest frame.

The relative energy spectrum $\frac{d\sigma}{dE_{tn}}$ i.e. the distribution in relative energy $E_{tn}$ between the charged fragment and the neutron, is derived from

$$E_{tn} = \frac{m_t + m_n}{2m_t m_n}\mathbf{p}_{tn}^2. \tag{2}$$

The experimental relative energy spectrum for $^4$H ($t$+$n$ channel) is shown in Fig. 1.

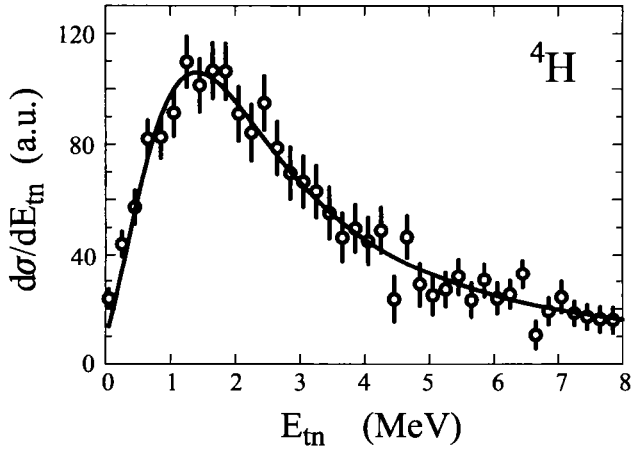


Fig. 1. The relative energy spectrum of the $t$+$n$-system obtained in one-proton knockout reactions with a $^6$He beam at 240 MeV/u impinging on a carbon target. The experimental data are shown as circles with statistical uncertainties. The solid line is the result of a fit using a Breit Wigner expression, convoluted with the response of the experimental setup, with $E_R$ = 2.67(9) MeV, $\Gamma^{obs}$ = 3.28(12) MeV (see text).

The most relevant information of the T=1, A=4 nuclei comes from Coulomb-corrected charge-independent R-matrix analysis [4]. The derived R-matrix parameters account well for the $N$-$^3$H elastic scattering cross section and coherent scattering length. The $I^\pi$=2$^-$ ground state of $^4$H is overlapping with the 1$^-$ first excited state, both are about 3 MeV broad and predicted to be separated by only 300 keV [4]. The states have the same structure, i.e. a neutron in the $p_{3/2}$ shell coupled to the triton core, and since in $^6$He the two neutrons are predominantly occupying the $p_{3/2}$ shell [19], the sudden one-proton knockout from $^6$He as studied here is expected to populate both the 2$^-$ and 1$^-$ states in $^4$H. Thus, only one peak is expected in the $\frac{d\sigma}{dE_{tn}}$ experimental spectrum,

since both states are much broader than their separation in excitation energy ($\sim$ 300 keV). The higher lying $0^-$ and $1^-$ states arising from a neutron in the $p_{1/2}$ shell coupled to the triton will only be weakly populated due to the small weight of the $(p_{1/2})^2$ configuration in the ground state of $^6$He. The $t$+$n$ spectrum reveals only one peak and may also be considered as evidence for a sudden proton knockout mechanism.

The experimental distribution can almost perfectly be fitted by using a single Breit-Wigner shaped resonance. To compare with the obtained data the following parameterization was used [20]

$$\frac{d\sigma(E)}{dE} \sim \frac{\Gamma}{(E_\lambda - \Delta_l - E)^2 + \frac{1}{4}\Gamma^2} \tag{3}$$

$$\Gamma = 2\gamma^2 P_l(E) = 2\gamma^2 \frac{\mathbf{k}R}{F_l^2 + G_l^2} \tag{4}$$

$$\Delta_l = \gamma^2 S_l(E) = \gamma^2 \mathbf{k}R \frac{F_l F_l' + G_l G_l'}{F_l^2 + G_l^2} \tag{5}$$

Here, the Coulomb functions $F_l$ and $G_l$ are the regular and irregular solutions of the Schrödinger equation where $R$ is the channel radius and $E$ the relative energy between neutron and triton. $S_l(E)$ is the channel shift function and $P_l(E)$ the channel penetrability function. $E_\lambda$ is the formal energy of the resonance and $\Gamma$ is its width, $\gamma^2$ is the reduced width. The resonance energy $E_R$ is defined as that center-of-mass energy where $E_\lambda - \Delta_l - E$ is equal to zero. The observed width is determined using the expression

$$\Gamma^{obs} = \frac{\Gamma}{1 + \gamma^2 \left(\frac{dS}{dE}\right)|_{E_R}}. \tag{6}$$

The full drawn curve in Fig. 1 was obtained from a fit with $l = 1$ using a channel radius $R = 4$ fm [21], resulting in the following parameters: $E_\lambda$=3.56(9) MeV, $E_R$=2.67(9) MeV, $\gamma^2$=2.73(10) MeV and $\Gamma^{obs}$=3.28(12) MeV. The given uncertainties are statistical, and the systematic uncertainties for the resonance position $E_R$ and the width $\Gamma^{obs}$ are $\pm$0.3 MeV and $\pm$0.2 MeV, respectively.

The extracted parameters are in agreement with experiments where $^4$H was studied in different nuclear reactions by the missing mass method (see review [4]). However, one notes that the maximum in the measured relative energy spectrum (Fig. 1) is at about 1.6 MeV of the $t$-$n$ relative energy, while the experimental excitation function for $n$-$t$ elastic scattering is peaked at 2.6 MeV [22]. In order to understand this effect, the elastic scattering cross section was calculated using the R-matrix expression (formulae 1.14 on p. 322

in Ref. [20]) using the resonance parameters obtained in the present work, and without any additional parameters the peak position given in Ref. [22] could be reproduced. The interference between potential and resonance scattering is the reason for the shift of the maximum, and thus the position of the maximum in the experimental distribution is dependent on the reaction mechanism. The effect is most pronounced in connection with broad resonances and might be the reason for the scatter of the experimental data on the resonance position. In some cases, the $^4$H resonance position was only determined from the maximum in the measured spectrum [4].

### *3.2 The $^5$H case*

We now turn to the $^5$H case where two neutrons are registered in coincidence with a triton. Jacobi coordinates are generally used analyzing three-body systems, where the dynamics of the system are determined by the relative momenta in the subsystems. The two different Jacobi coordinate systems used to describe the $t$+$n$+$n$ system are illustrated in Fig. 2.

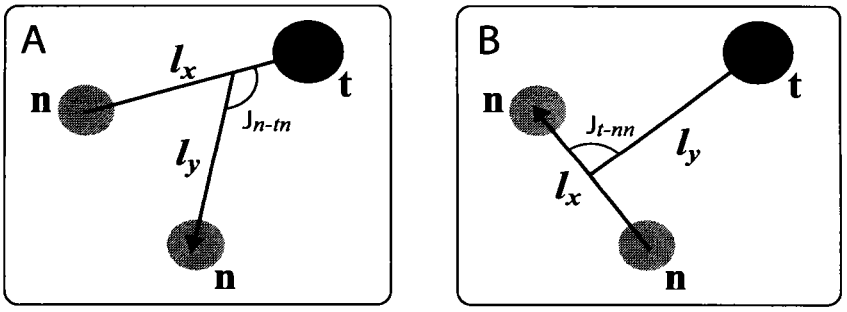


Fig. 2. The two different (**A**: $n-tn$ and **B**: $t-nn$) Jacobi-momentum coordinate systems used for analyzing the data.

In the set of Jacobi coordinates which is marked by **A** in Fig. 2 the $t$+$n$+$n$ system is described by the relative momenta between the triton and one of the neutrons $\mathbf{p}_{tn_1}$ and relative momenta between their center of mass and the second neutron $\mathbf{p}_{n_2-tn_1}$:

$$\begin{cases} \mathbf{p}_{tn_1} = \frac{\mathbf{p}_t m_n - \mathbf{p}_{n_1} m_t}{m_t + m_n} \\ \mathbf{p}_{n_2-tn_1} = \frac{\mathbf{p}_{n_2}(m_n+m_t) - (\mathbf{p}_{n_1}+\mathbf{p}_t) m_n}{m_t + 2m_n} \\ \mathbf{p}_{n_1} + \mathbf{p}_{n_2} + \mathbf{p}_t = \mathbf{p}_{^5\mathrm{H}} \end{cases} \tag{7}$$

Here, the triton momentum ($\mathbf{p}_t$) and neutron momenta ($\mathbf{p}_{n_1}$ and $\mathbf{p}_{n_2}$) are defined in the projectile rest frame.

The relative energy spectrum, $\frac{d\sigma}{dE_{tnn}}$, in the three-body system $t$+$n$+$n$, i.e. the distribution of the total kinetic energy in the three body system $E_{tnn}$, is obtained from the relative momenta $\mathbf{p}_{tn_1}$ and $\mathbf{p}_{n_2-tn_1}$

$$E_{tnn} = \frac{(m_t + m_n)\mathbf{p}^2_{tn_1}}{2m_n m_t} + \frac{(m_t + 2m_n)\mathbf{p}^2_{n_2-tn_1}}{2m_n(m_t + m_n)}, \tag{8}$$

the corresponding $^5$H spectrum is shown in Fig. 3. A similar expression can also be derived in system **B**.

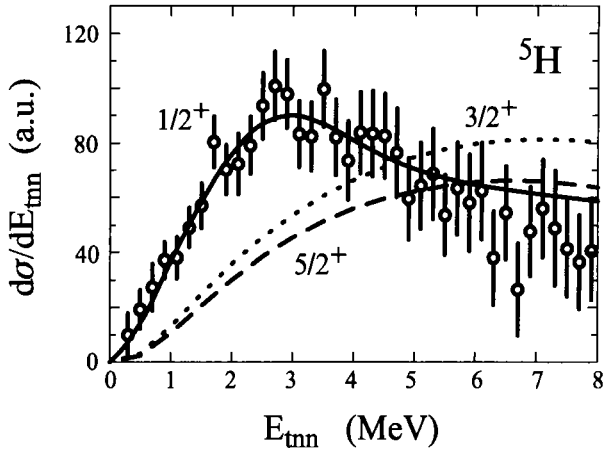


Fig. 3. The relative energy spectrum of the $t$+$n$+$n$-system obtained in one-proton knockout reactions with a $^6$He beam at 240 MeV/u impinging on a carbon target. The experimental data are shown by circles with statistical uncertainties. The solid line is the result of a three-body microscopic calculation for the $t$+$n$+$n$ system, assuming $I^\pi = 1/2^+$ [2], the dotted and dashed line correspond to the $3/2^+$ and $5/2^+$ state respectively.

A conventional analysis using a Breit-Wigner formula, as was carried out for the $^4$H case, is not appropriate to analyze few-body systems. The observed structure (Fig. 3) exhibits a width of about 6 MeV (FWHM) and, as previously discussed, the maximum of the spectrum, at about 3 MeV cannot be interpreted directly as the resonance position. Therefore, as a first step, the spectrum is compared with calculations made within a strict three-body $t + n + n$ dynamics [2]. Configurations corresponding to $I^\pi = 1/2^+$, $3/2^+$ and $5/2^+$ states in $^5$H are used. As can be seen in Fig. 3, good agreement is achieved between experimental data and the shape of the calculated $I^\pi = 1/2^+$ state, which is the most probable ground state configuration as discussed earlier. Note, that the reason for the relatively narrow width as compared with the calculated decay through the di-neutron channel, is due to the three-body nature of the state [2].

## 4 Energy and angular correlations in the $t$+$n$+$n$ system

### *4.1 Combinatorial correlation functions*

In order to reveal correlation effects between the different fragments in the $t$+$n$+$n$ relative energy spectrum (Fig. 3) we will use the mixed-event method. This method is frequently used while analyzing elementary particle physics experiments to estimate the background from particles which may be decay products of resonances (see e.g. [23–25]). The method has also been used successfully for the search of two particle resonances in fragmentation reactions [15,26].

The $^5$H relative energy spectrum calculated using equation (8), results from the three momenta $\mathbf{p}_t$, $\mathbf{p}_{n_1}$ and $\mathbf{p}_{n_2}$, measured in coincidence. Using the same equation (8) but taking all three momenta from different events, the correlations between fragments in the calculated relative energy spectrum are washed out. A spectrum created this way can thus be used as a reference to reveal correlation effects between the fragments.

The correlations between one neutron and the triton are preserved when the momenta of $\mathbf{p}_t$ and $\mathbf{p}_{n_1}$ (or $\mathbf{p}_{n_2}$) are taken from the same event. The deviations from unity of the ratio ( $\mathcal{R}_{tn}$ ) of a spectrum so created to the reference spectrum would reveal the $t$-$n$ correlations. In addition, the $n$-$n$ correlations are preserved when momenta $\mathbf{p}_{n_2}$ and $\mathbf{p}_{n_1}$ are taken from the same event and deviations from unity of the ratio ( $\mathcal{R}_{nn}$ ) of this spectrum to the reference spectrum likewise demonstrate this effect. The $\mathcal{R}_{nn}$ and $\mathcal{R}_{tn}$ correlation functions are shown in Fig. 4 as data points with indication of statistical uncertainties. For a more profound understanding and interpretation of $\mathcal{R}_{tn}$ and $\mathcal{R}_{nn}$, a simulation was performed. Therein the $t$+$n$+$n$ relative energy distribution was adopted from experimental results, i.e. the one displayed in Fig. 3. The relative energy was then shared by the three particles according to their phase space and instrumental resolutions were folded in. From these simulated data, $\mathcal{R}_{tn}$ and $\mathcal{R}_{nn}$ were built in an identical manner as the experimental data and are shown in Fig. 4 as solid lines. The deviation between the simulated and experimental correlation functions $\mathcal{R}_{nn}$ and $\mathcal{R}_{tn}$ show that the experimental data reveal additional correlations, which cannot be explained merely by conservation laws.

As can be seen (Fig. 4 left) the $n$-$n$ correlations in the experimental distribution are the most prominent, resulting to an enhancement of the $^5$H relative energy spectrum at energies below 2 MeV. The $t$-$n$ correlations (Fig. 4 right) suppress the low energy part of the spectrum giving a more narrow distribution in comparison with the totally mixed spectrum. The decrease in $\mathcal{R}_{tn}$

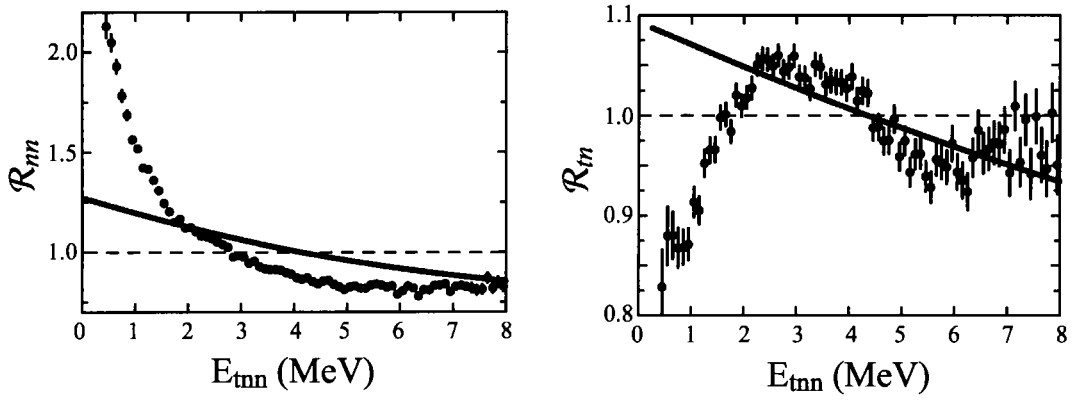


Fig. 4. Correlation functions obtained by an event-mixing method. The circles show the experimental correlation functions while the solid lines correspond to correlations reflecting only energy and momentum conservation in the decaying three-body system (see text).

at low energy can be attributed to a repulsive $t$-$n$ interaction at low relative energies.

Qualitatively, the shape of the $^5$H resonance is only reflected in $\mathcal{R}_{tn}$ but not in $\mathcal{R}_{nn}$. The interpretation of the observed effect is that the di-neutron decay is dominating at low energy and, as discussed in the Introduction, counteracts a narrow $^5$H resonance, while the sequential neutron emission determines the spectrum at higher energies. Therefore both $n$-$n$ and $t$-$n$ correlations are of vital importance for the $^5$H resonance.

### *4.2 Three-body correlations*

In this section further energy and also angular correlations will be discussed in order to obtain quantitative estimates.

The three body configuration is determined by the angle ($\vartheta$) between the Jacobi momenta, by the total energy of the three-body system and by the energy shared by corresponding pair of particles (see Fig. 2). The variable $\varepsilon_{tn} = E_{tn}/E_{tnn}$ in Jacobi set **A** or variable $\varepsilon_{nn} = E_{nn}/E_{tnn}$ in Jacobi set **B** (Fig. 2) determines the ratio of relative energy for each pair of particles, where evidently $0 \leq \varepsilon \leq 1$.

The corresponding experimental distributions for the variables $\varepsilon$ and $\vartheta$ in the two Jacobi systems are shown in Fig. 5 where (1) and (3) are shown in Jacobi configuration **A** ($n - tn$) and, (2) and (4) in configuration **B** ($t - nn$). The

distributions were constructed from events restricted to the vicinity of the peak position ($E_{tnn}\sim$ 1-5 MeV) in the $^5$H relative energy spectrum.

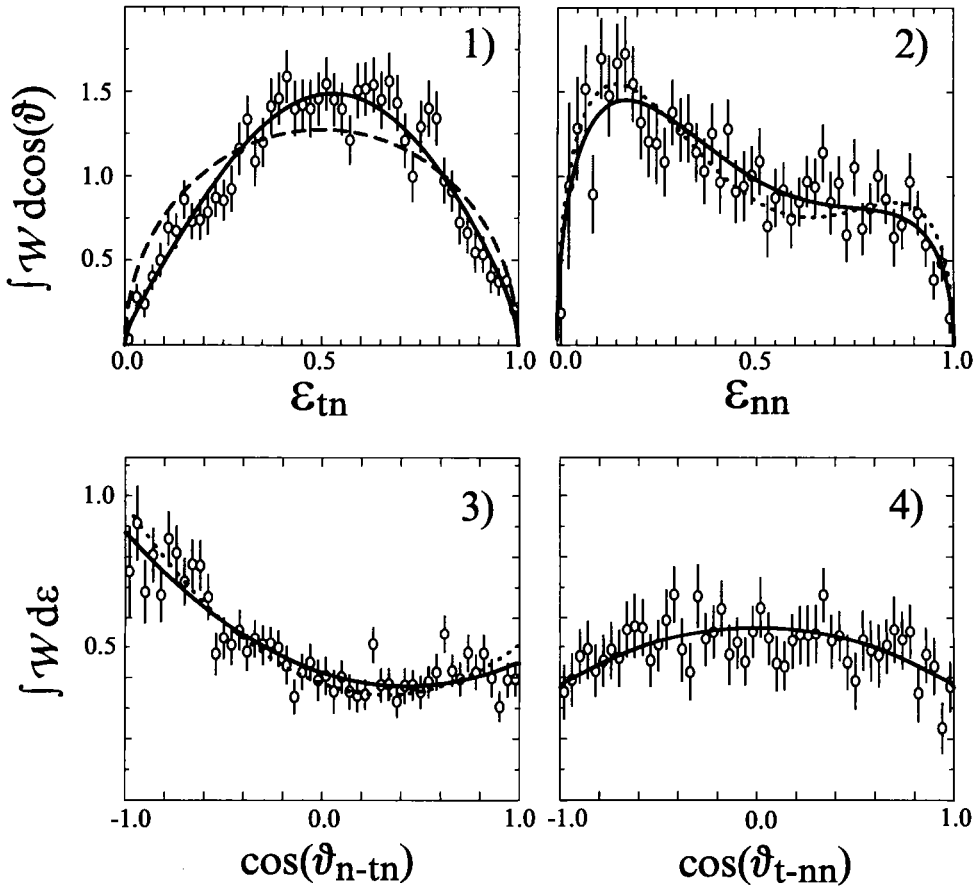


Fig. 5. Energy and angular correlations in two different Jacobi coordinate systems. Figures (1) and (3) refers to in Jacobi configuration **A** ($n - tn$), (2) and (4) in configuration **B** ($t - nn$). The experimental data are shown as open circles with statistical uncertainties. The dashed line in (1) corresponds to a conventional phase space distribution. The solid lines represent the fit to the distributions on the basis of expansion on hyperspherical harmonics after convolution with the detector response. The dotted lines shown in (2,3) correspond to the same fit but the fit functions were not distorted by the experimental resolution.

The energy distribution shown in Fig. 5(1) looks at first glance similar to that expected from a conventional phase space distributions

$$d\sigma/d\varepsilon \sim \sqrt{\varepsilon(1-\varepsilon)}. \tag{9}$$

However, this phase space distribution cannot reproduce the experimental

data, see dashed line in Fig. 5(1).

For a three-body system, where no narrow resonances exist in any of the binary subsystems, the following equation holds [27]

$$d\sigma/d\varepsilon \sim \varepsilon^{l_x+\frac{1}{2}} (1-\varepsilon)^{l_y+\frac{1}{2}} \tag{10}$$

where $l_x$ and $l_y$ are the angular momenta in the $t$-$n$ and $n$-$tn$ subsystems, respectively. The experimental distribution shown in Fig. 5(1) can be reasonably well approximated by equation (10) with $l_x = l_y = 1$ indicating that the main contribution to the final state wave function mainly stems from $p$-shell configurations [2].

The strong $n$-$n$ interaction can again be observed, first in the asymmetric energy distribution shown in Fig. 5(2), and second in the angular distribution in Fig. 5(3): the two neutrons preferably have low relative energy and are emitted in opposite direction to the charged fragment. Most noticeably, the asymmetry in the distribution in Fig. 5(3) indicates a strong interference of waves with different parity. As a next step, in order to clarify the situation further, a robust analysis was made leading to more quantitative results.

As mentioned in the Introduction, the structure of $^5$H is expected to be similar to that of $^6$He. The properties of the $^6$He ground state have been carefully studied using HH calculations for this three-body system (see Ref. [28] and references therein). A remarkable feature is that the $^6$He ground-state wave function essentially, is composed of very few components, which correspond to the lowest momenta in the three-body system. The components with hypermomentum K = 0 and 2 and with relative angular momenta $l_{x(y)} \leq 1$, between the fragments exhaust 97% of the norm of the $^6$He ground state wave function [28]. One would expect that in the one-proton knockout from $^6$He (in the sudden approximation) the same configuration would be preserved in the residual nucleus $^5$H. However, final state interactions of the fragments passing through centrifugal barriers during the decay process, may change relative contributions of the components. To analyze the experimental data, a method was used as proposed in Ref. [29], which is based on a fitting procedure using the series expansion of the final state wave function into the hyperspherical functions. The HH are the eigenfunctions of the angular part of the Schrödinger equation in the six dimensional space. The proposed method thus represents a generalization of the Legendre polynomial expansion known from two-body systems to the case of the three-body systems.

Here, only components dominating the $^6$He ground state are used: i.e. K =

[2] This first order approximation will be used further in the discussion of the changes in the $t$+$n$ relative energy spectrum under influence of the second neutron, see Appendix A.

0,2 and $l_{x(y)} = 0,1$. Further, an approximation where the core spin is not included is used, which implies, that the properties of the system $n$-$n$-core are governed by their relative motion. The expansion is characterized by a set of complex amplitudes $C_{SKl_xl_y}$ for the respective harmonics, (namely, $C_{0000}$, $C_{0200}$, $C_{0211}$ and $C_{1211}$), where $S$ is the total spin of the two neutrons, $K$ is the hypermomentum, and $l_{x(y)}$ are the relative angular momenta in the corresponding Jacobi coordinate system. Details are given in Ref. [29].

The explicit expression for the probability distribution $\mathcal{W}$ used to fit the data, valid in both Jacobi sets, has the following form

$$\mathcal{W}(\varepsilon,\vartheta) = \frac{4}{\pi}\sqrt{\varepsilon(1-\varepsilon)} \cdot \left\{ \left| C_{1211} \right|^2 8\varepsilon(1-\varepsilon)\sin^2\vartheta \right. \tag{11}$$
$$\left. + \left| C_{0000} - C_{0200}\, 2(2\varepsilon-1) + C_{0211}\, 4\sqrt{\varepsilon(1-\varepsilon)}\cos\vartheta \right|^2 \right\},$$

where $\mathcal{W}(\varepsilon,\vartheta)$ is normalized to unity.

The transformation from Jacobi system **B** to system **A** (amplitudes $C \rightarrow C'$) is provided by Raynal-Revai coefficients [30]. The explicit transformation of the amplitudes gives:

$$\begin{cases} C'_{0000} = C_{0000} \\ C'_{0200} = -\sqrt{\frac{15}{16}}\, C_{0211} - \sqrt{\frac{1}{16}}\, C_{0200} \\ C'_{0211} = -\sqrt{\frac{1}{16}}\, C_{0211} + \sqrt{\frac{15}{16}}\, C_{0200} \\ C'_{1211} = C_{1211} \end{cases} \tag{12}$$

The symmetry properties are more easily discussed in Jacobi system **B** (Fig. 2), where the antisymmetrization of the wave function with respect to the two neutrons results in $C_{0211} = 0$. Moreover, an interference effect causing asymmetric distributions in this system can only exist between the harmonics with $C_{0000}$ and $C_{0200}$ and is determined by the their phase difference $\beta_{0200}$ [3]. And as can be obtained from the transformation (12), the phase differences $\alpha_{SKl_xl_y}$ in system **A** are fixed by the phase difference $\beta_{0200}$ in system **B**, namely

[3] All phase differences mentioned hereafter will be determined relative to $C_{0000}$ in system **B**.

$\alpha_{0211} = \alpha_{0200} + \pi = \beta_{0200}$. In system **B**, only one distribution reveals asymmetry, Fig. 5(2), and $\beta_{0200}$ is associated with this. In system **A** though, an asymmetry can be seen in two distributions, Fig. 5(1) and Fig. 5(3). The phase difference connected with these are $\alpha_{0200}$ and $\alpha_{0211}$, respectively.

Two different fits were made, where the first fit was used to check the consistency of the model applied. All parameters were extracted using the probability distribution $\mathcal{W}$ from equation (11) to simultaneously fit the four distributions shown in Fig. 5. The experimental resolution was taken into account.

In the first fit, all seven parameters were kept free ($C_{0200}$, $C_{0211}$, $C_{1211}$, $\beta_{0200}$, $\beta_{0211}$, $\alpha_{0200}$, $\alpha_{0211}$). The result for the corresponding system is shown in row $B^1$ and $A^1$ of Table 1. Remarkably, in system **B**, $|C_{0211}|^2$ is obtained equal to zero within statistical accuracy. In addition, within an accuracy of a few degrees the relation between the phases mentioned above is fulfilled, note however that $\beta_{0211}$ remains statistically undetermined. Thus, this fitting procedure gives evidence that the basic properties of the three-body system are well reproduced and demonstrate a high confidence level for the extracted parameters, see Appendix B for more details.

Table 1
Weights $|C_{SKl_xl_y}|^2$ of the different HH components (given in percent), and phases ($\alpha$ and $\beta$, given in degrees) obtained from two different fits of the experimental data of $^5$H in configuration **B** ($t-nn$), and **A** ($n-tn$), see text for further explanation. The errors given are statistical. Unconstrained parameters are shown in bold fonts.

| Fit | $\mid C_{0000} \mid^2$ | $\mid C_{0200} \mid^2$ | $\mid C_{1211} \mid^2$ | $\mid C_{0211} \mid^2$ | $\beta_{0200}$ | $\beta_{0211}$ |
|---|---|---|---|---|---|---|
| $B^1$ | 17(4) | **46(3)** | **37(5)** | **0.02(9)** | **60(3)** | **0(180)** |
| $B^2$ | 18(3) | **45(2)** | **37(4)** | 0.0 | **61(2)** | - |
| Fit | $\mid C'_{0000} \mid^2$ | $\mid C'_{0200} \mid^2$ | $\mid C'_{1211} \mid^2$ | $\mid C'_{0211} \mid^2$ | $\alpha_{0200}$ | $\alpha_{0211}$ |
| $A^1$ | 17(4) | 2.9(1) | 37(5) | 43(3) | **243(9)** | **61(3)** |
| $A^2$ | 18(3) | 2.9(1) | 37(4) | 42(2) | 241(2) | 61(2) |

The second fit was made with three free parameters, $C_{0200}$, $C_{1211}$ and $\beta_{0200}$. All the other parameters are determined either by symmetry properties or transformation characteristics discussed above, i.e. $C_{0211}$ is fixed at zero and the phases $\alpha_{0211} = \alpha_{0200} + \pi = \beta_{0200}$. The result is shown in the rows $B^2$ and $A^2$ of Table 1, and its correspondence with the experimental data is demonstrated by solid lines in Fig. 5. For all angular and energy distributions the fit can reproduce the experimental data with good accuracy, the reduced overall $\chi^2$ is close to one ($\sim 0.94$). The dotted lines in Fig. 5 show the corresponding distributions which are not corrected for experimental resolution.

The configurations with $C_{0000}$ and $C_{0200}$ directly result in a total spin $I^\pi = 1/2^+$ for the $t$+$n$+$n$ system. Some portion of the $C_{1211}$ component can also

be assigned to this spin and parity. From the weights given in Table 1, the conclusion is thus that the $I^{\pi} = 1/2^{+}$ state in $^{5}$H system is populated with probability larger than 65%. Further, a transformation to Jacobi system **A** results in about 80% configuration with the two neutrons in the $p$-shell.

### *4.3 Resemblance between $^{5}H$, $^{6}He$ and $^{6}Be$ structures*

A comparison between the experimental results for the $^{5}$H structure revealed in the decay products and the microscopical three-body calculations for $^{6}$He [28] is demonstrated in the first two rows of Table 2. The results are shown for the Jacobi system **B**.

It should be noted that the weight of the configuration with $K = 0$ in $^{5}$H is significantly larger than that calculated for $^{6}$He. The increase of this component is expected due to the suppressed three-body centrifugal barrier determined by $K$ in this decay channel. Further, the increase of the $K = 0$ contribution can be attributed to the $n$-$n$ interaction in the final state. The effects of the $n$-$n$ interaction are well pronounced even though the experimental phase difference $\beta_{0200}$ results in a decrease of the interference term compared with the $^{6}$He calculation.

Table 2
Weights $|C_{SKl_xl_y}|^2$of the different partial waves (given in percent), obtained from the fit of the experimental data of $^{5}$H in Jacobi set **B**. The experimental $^{6}$Be ground state data are taken from Ref. [29] and the theoretical calculations for the $^{6}$He ground state wave function are taken from Ref. [28]. The phases $\beta$ are given in degrees.

| Config. | $\mid C_{0000} \mid^2$ | $\mid C_{0200} \mid^2$ | $\mid C_{1211} \mid^2$ | $\beta_{0200}$ | Reference |
|---|---|---|---|---|---|
| $^{6}$He | 4 | 78 | 15 | 0 | [28] *theo.* |
| $^{5}$H | 18(3) | 45(2) | 37(4) | 61(2) | present *exp.* |
| $^{6}$Be | 6(5) | 44(12) | 50(17) | 70 | [29] *exp.* |

Compared to $^{6}$He, the component, with S = 1 and $K = 2$ is also significantly larger in the experimental $^{5}$H data. The effect might be attributed to the $t - n$ final state interaction. For $jj$-coupling, the S=1 component, which is directly related to $C_{1211}$, is about 33% in the pure $(p_{3/2})^2$ configuration. The transformation of the experimental data from the LS coupling scheme used in the current analysis procedure to jj-coupling remains ambiguous as far as the phase of $C_{1211}$ cannot be determined from the experimental data. A transformation assuming the phase shift taken from the $^{6}$He calculation [28] results in about 80% of the weight of configuration with the two neutrons in $p_{3/2}$-shell and only 1% left for a possible $p_{1/2}$-shell admixture.

Thus, a good resemblance between the $^6$He wave function and the structure of the $t$+$n$+$n$ system is found, and the observed differences are qualitatively explained by the decay processes of the preformed $^5$H.

The unstable $^6$Be nucleus is a mirror nucleus to $^6$He and is expected to have a similar structure. The correlation of the $^6$Be decay products has been studied experimentally by the HH expansion method [29], and the parameters derived are shown in Table 2. Even though $^6$Be and $^5$H are very different[4], the similarities between the data from these two experimental results are remarkable and reflect the similarities in the structure of these nuclei.

The experimental results given in this section indicate that the expected configuration [2,3] for the $^5$H ground state is strongly populated in the reaction. However, narrow resonance structures were not observed. The following fact should be taken into consideration: $^4$H is unstable relative to neutron emission by 2.7 MeV, and thus, ignoring the neutron pairing energy, $^5$H would be unstable by 5.4 MeV. The pairing effects should be less pronounced for a diluted $^5$H system compared to that for $^6$He, thus the neutron pairing energy in $^6$He (2.75 MeV) may be considered as an upper limit for the one in $^5$H. The lowest value for the position of the $^5$H resonance above $t$+$n$+$n$ threshold would therefore be 2.6 MeV. The observed peak position in the $^5$H relative energy spectrum is only 0.5 MeV above this value and thus in good agreement with this estimate. All experimental evidence presented in this section together with the theoretical calculations illustrated in Fig. 3 indicate that the observed broad resonance is due to the $^5$H ground state.

## 5 Summary and conclusion

The resonances in the $t$+$n$ and $t$+$n$+$n$ systems have been investigated in the one-proton knockout channel with a $^6$He beam impinging on a carbon target with the energy 240 MeV/u. The nucleon knockout is the dominant reaction mechanism at this energy. The knockout mechanism of the reactions manifested in the shape of the fragment momentum distributions, in the large probability for two neutrons having similar momenta, and in the energy and angular correlations in the $t$+$n$+$n$ system.

The data obtained for the $t$+$n$ system are consistent with a $^4$H resonance state at $E_R$=2.67(31) MeV, and of width $\Gamma^{obs}$=3.28(23) MeV. This result is in reasonable agreement with experiments where $^4$H has been studied in different types of nuclear reactions using the missing mass method. The $^4$H resonance

[4] The $^6$Be$_{(gs)}$ resonance width is about 90 keV, while the $^5$H resonance, if it exists, is several MeV broad.

is broad and the apparent peak position in the experimental distributions depends on the reaction mechanism. Thus, a theoretical analysis is necessary to derive the resonance energy.

A broad distribution centered at 3 MeV with a width in the order of 6 MeV (FWHM) is observed in the $t$+$n$+$n$ relative energy spectrum. This distribution is well described by microscopic dynamical calculations in a three-body continuum [2] with $I^\pi = 1/2^+$. The correlation functions constructed by the mixed event method reveal the importance of both $n$-$n$ and $t$-$n$ correlations. The experimentally determined angular and energy correlations between fragments were analyzed using the method of hyperspherical harmonic expansion and the weights of the partial waves in the final state were determined. The population of the $I^\pi = 1/2^+$ state with two neutrons in the $p$-shell was found to be dominant. The present result, taking into account the broadness of the observed structure, is in agreement with the results published in Refs. [5,8]. However, no evidence for a narrow resonance in the $t$+$n$+$n$ system as previously reported e.g. in [7,6] was observed. Note also that the reaction chosen here populates preferentially states with well pronounced $t$+$n$+$n$ cluster structure and the probability to populate $^5$H with a different internal structure is very low. A narrow $^5$H resonance of a different structure may exist, e.g. a five-body compound configuration where the triton core is dissolved by the valence neutrons. In this case, the only energetically possible decay channel $t$+$n$+$n$ would be structurally suppressed and a narrow $^5$H resonance could be formed. Some arguments for this may be found in recent calculations treating $^5$H as a system of five nucleons [31], see also Ref. [32] where a $d$+$Xn$ structure of $^4$H and $^6$H is discussed.

## 6 Acknowledgement

The authors acknowledge with gratitude useful discussions with L.V. Grigorenko and M.V. Zhukov. We are also grateful to N.B. Shulgina for providing the numerical results of her calculations.

This work was supported by the BMBF under Contracts 06 DA 820, 06 OF 112 and 06 MZ 864 and by GSI via Hochschulzusammenarbeitsvereinbarungen under Contracts DA RICK, OF ELZ, MZ KRK and partly supported by the Polish Committee of Scientific Research under Contract PBZ/PB03/113/09, EC under contract ERBCHGE-CT92-0003, CICYT under contract AEN92-0788-C02-02 (MJGB) and RFBR grant No. 01-02-16685. One of us (B.J.) acknowledges the support through an Alexander von Humboldt Research Award.

## Appendix A

### The influence of the second neutron on the $t$+$n$ relative energy spectrum

In this section we will compare the $t$+$n$ relative enegy spectra obtained with two different choices of the relative momenta between the two neutrons.

In the first case, the relative enegy spectrum was obtained from events where one of the two neutrons did not fall into the LAND acceptance, previously shown in Sect. 3, Fig. 1. Thus the undetected neutron was well separated in momentum space from the detected neutron and triton. The fit to the obtained spectrum was done using a Breit-Wigner formula and is represented by the solid line in Fig. 6.

In the second case, the $t$+$n$ relative enegy spectrum was reconstructed from events where both neutrons have transverse momenta smaller than 60 MeV/c, and both were detected in LAND. The result is shown in Fig. 6 as a histogram. As can be seen, the latter is shifted towards lower energies by about 1 MeV.

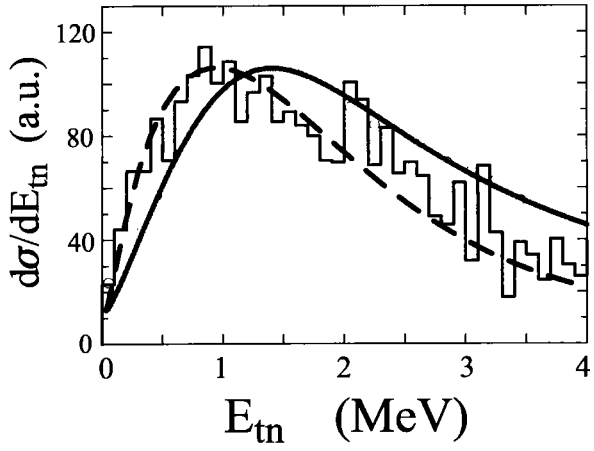


Fig. 6. The relative enegy spectrum of the $t$+$n$ system obtained when two neutrons were detected in LAND in coincidence with the triton shown as a histogram. The solid line demonstrates the Breit-Wigner fit to the measured $^4$H relative enegy spectrum obtained when one of the two neutrons fell outside the LAND acceptance. The dashed line is the result of calculation assuming that neutron and triton are decay products of $^5$H.

The dashed line displayed in Fig. 6 shows the result of a calculation obtained with the assumptions that (i) both, neutron and triton, are decay products of the $^5$H and that (ii) the decay probability is proportional to the final state phase space. The final state phase space can be approximated by Equation (10) where $l_x = 1$ and $l_y = 1$. The differential cross section $d\sigma/dE_{tn}$ is then calculated using:

$$\frac{d\sigma}{dE_{tn}} \sim \int_{E_{tn}} \frac{d\sigma}{dE_{tnn}} \frac{\sqrt{E_{tn}^3 (E_{tnn} - E_{tn})^3}}{E_{tnn}^4} dE_{tnn} \tag{13}$$

Here, $d\sigma/dE_{tnn}$ is taken as the experimental relative enegy spectrum of $^5$H and a numerical integration is performed. Note, we have already shown in the previous sections, that no narrow resonances can be found in the binary subsystems of $^5$H, neither in the $t + n$ nor in the $n + n$ channel which is a prerequisite for the validity of equation (10).

The agreement of the calculation with the experimental distribution therefore supports the assumption that, if all three particles are close in momentum space, both neutrons and the triton can be attributed to be $^5$H decay products.

## Appendix B

### Confidence level of the parameters obtained in the fitting procedure.

As discussed in Section 4, the experimental distributions were fitted by the expansion with a restricted set of hyperspherical harmonics and the weights of the partial waves in the $t + n + n$ final state wave function were obtained. The systematical uncertainties of the parameters derived are mainly connected with the contribution from higher harmonics. This contribution is expected to be on a level of a few percent to the norm of the probability distribution $\mathcal{W}$ determined by equation (11). We discuss here the first fit that was made to check the validity of the applied model to describe the experimental data and where the basic basic symmetry properties of the $t$+$n$+$n$ system were not explicitly taken into account. The antisymmetrization of the wave function with respect to the two neutrons implies that the weight of the $C_{0200}$ harmonic should be equal to zero in Jacobi system **B** and the phase differences in Jacobi system **A** are determined by the single phase differences in Jacobi system **B**: $\alpha_{0211} = \alpha_{0200} + \pi = \beta_{0200}$. This strict statement is only true if $t$+$n$+$n$ is an isolated three-body system. The symmetry properties of the three-body system are also of vital importance for the understanding of the reaction mechanism. The confidence level of the result obtained is discussed below.

The left part of Fig. 7 demonstrates a contour plot showing constant $\chi^2$ levels and its dependence on the amplitude modulus $C_{0211}$ and $C_{0200}$ in system **B**. For each point on the contour lines all remaining five parameters were varied. A distinct minimum in $\chi^2$ is obtained for the parameters given in Table 1, Section 4. The projection of the area inside $\chi^2_{min} + 1$ in the figure to the respective axis reflects one standard deviation of each individual parameter. The projection of the area inside $\chi^2_{min} + 2.5$ to the x-axis restricts the contribution

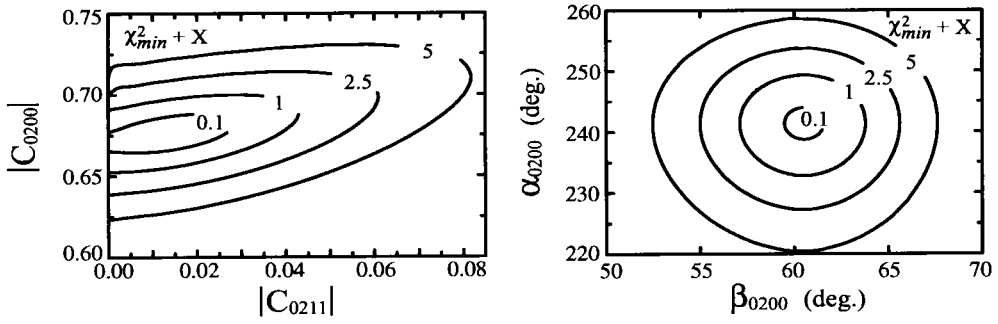


Fig. 7. Contour plot showing the dependence of $\chi^2$ for the amplitudes $C_{0211}$ and $C_{0200}$ in system **B** and phases $\alpha_{0200}$ and $\beta_{0200}$. For each point on the contour lines all remaining parameters were varied.

of the forbidden $C_{0211}$ harmonic to less than 0.4% on an approximately 90% confidence level [33,34].

The right part of Fig. 7 demonstrates a contour plot showing constant $\chi^2$ levels and its dependence on the phases $\beta_{0200}$ and $\alpha_{0200}$. The parameter $C_{0211}$ was set to zero and for each point on the contour lines all four remaining parameters were varied. A distinct minimum in $\chi^2$ is obtained for the parameters given in Table 1, Section 4. The projection of the area inside $\chi^2_{min}+1$ in the figure to the respective axis reflects one standard deviation of each individual parameter. The area inside $\chi^2_{min}+5$ shows the region of approximately 90% confidence level for the values of these two parameters simultaneously. As demonstrated in Fig. 7, the phase differences follows the relation $\beta_{0200} = \alpha_{0200} + \pi$. Note, that parameter $\alpha_{0200}$ is determined by the very small asymmetry which can be noticed in Fig. 5(1) and suffers most from the statistical uncertainties. Thus, the relation $\beta_{0200} = \alpha_{0211}$ is fulfilled with even higher accuracy.

As can be seen, the model used to fit the experimental data is consistent with the symmetry properties and transformation rules which are the characteristics of the $t$+$n$+$n$ system. As a conclusion, the weights of the partial waves in the $t$+$n$+$n$ final state wave function can be determined from the fit with a high confidence level. Besides, this result gives evidence that $t$+$n$+$n$ is a well isolated three-body system. Thus, one can assume for the reaction mechanism that the momentum of the $t$+$n$+$n$ center-of-mass reflects the internal momentum of the proton knocked out from $^6$He.

## References


[1] A.A. Ogloblin, Yu.E. Penionzhkevich, Treatise on Heavy-Ion Science, Vol. 8 p. 261, Ed.D.A. Bromley, Plenum Press NY, 1989

[2] N.B. Shulgina, B.V. Danilin, L.V. Grigorenko, M.V. Zhukov, J.M. Bang, Phys. Rev. **C62** (2000) 014312

[3] P. Descouvemont, A. Kharbach, Phys. Rev. **C63** (2001) 027001

[4] D.R. Tilley, C.M. Cheves, J.L. Godwin, G.M. Hale, H.M. Hofmann, J.H. Kelley, C.G. Sheu, H.R. Weller, Nucl. Phys. **A708** (2002) 3
D.R. Tilley, H.R. Weller, G.M. Hale, Nucl. Phys. **A541** (1992) 1

[5] M.G. Gornov, Ju.B. Gurov, S.V. Lapushkin, P.V. Morohov, M.S. Padorin, N.O. Poroshin, V.A. Pechurov, B.G. Sandukovskii, M.V. Tel'kushev, B.A. Chernyshev, *LII meeting on Nuclear Spectroscopy and Nuclear Structure, June 18-22, 2002, Moscow, Russia*, Book of Abstracts (2002) p. 70

[6] A.A. Korsheninnikov, M.S. Golovkov, I. Tanihata, A.M. Rodin, A.S. Fomichev, S.I. Sidorchuk, S.V. Stepantsov, M.L. Chelnokov, V.A. Gorshkov, D.D. Bogdanov, R. Wolski, G.M. Ter-Akopian, Yu.Ts. Oganessian, W. Mittig, P. Roussel-Chomaz, H. Savajols, E.A. Kuzmin, E.Yu. Nikolsky, A.A. Ogloblin, Phys. Rev. Lett. **87** (2001) 092501

[7] G.M. Ter-Akopian, *VII International School Seminar, May 27 - June 1, 2002, Dubna, Russia*, Book of Abstracts (2002) p. 87

[8] D.V. Aleksandrov, E.Yu. Nikolsky, B.G. Novatsky, D.N. Stepanov, *Proc. Intern. Conf. on Exotic Nuclei and Atomic Masses (ENAM-95), June 19-23, 1995, Arles, France* (1995) p. 329

[9] P.G. Young, R.H. Stokes, G.G. Ohlsen, Phys. Rev. **173** (1968) 949

[10] D.V. Aleksandrov, E.Yu. Nikolsky, B.G. Novatsky, D.N. Stepanov, P. Bem, V. Burjan, J. Vincour, Z. Dlouhy, V. Kroha, D.S. Baiborodin, Yad. Fiz. **62** No 11, (1999) 1925; Phys. Atomic Nuclei **62** (1999) 1789

[11] K. Markenroth, M. Meister, B. Eberlein, D. Aleksandrov, T. Aumann, L. Axelsson, T. Baumann, M.J.G. Borge, L.V. Chulkov, W. Dostal, Th.W. Elze, H. Emling, H. Geissel, A. Grünschloss, M. Hellström, J. Holeczek, B. Jonson, J.V. Kratz, R. Kulessa, A. Leistenschneider, I. Mukha, G. Münzenberg, F. Nickel, T. Nilsson, G. Nyman, M. Pfützner, V. Pribora, A. Richter, K. Riisager, C. Scheidenberger, G. Schrieder, H. Simon, J. Stroth, O. Tengblad, M.V. Zhukov, Nucl. Phys. **A679** (2001) 462

[12] M. Meister, K. Markenroth, D. Aleksandrov, T. Aumann, L. Axelsson, T. Baumann, M.J.G. Borge, L.V. Chulkov, W. Dostal, B. Eberlein, Th.W. Elze, H. Emling, C. Forssén, H. Geissel, M. Hellström, R. Holzmann, B. Jonson, J.V. Kratz, R. Kulessa, Y. Leifels, A. Leistenschneider, I. Mukha, G. Münzenberg, F. Nickel, T. Nilsson, G. Nyman, A. Richter, K. Riisager,

C. Scheidenberger, G. Schrieder, H. Simon, O. Tengblad, M.V. Zhukov, Phys. Rev. Lett. **88** (2002) 102501

[13] B.V. Danilin, M.V. Zhukov, A.A. Korsheninnikov, L.V. Chulkov, Yad. Fiz. **53** (1991) 71; Sov. J. Nucl. Phys. **53** (1991) 45

[14] T. Aumann, D. Aleksandrov, L. Axelsson, T. Baumann, M.J.G. Borge, L.V. Chulkov, J. Cub, W. Dostal, B. Eberlein, Th. W. Elze, H. Emling, H. Geissel, V. Z. Goldberg, M. Golovkov, A. Grünschloß, M. Hellström, K. Hencken, J. Holeczek, R. Holzmann, B. Jonson, A. A. Korsheninnikov, J. V. Kratz, G. Kraus, R. Kulessa, Y. Leifels, A. Leistenschneider, T. Leth, I. Mukha, G. Münzenberg, F. Nickel, T. Nilsson, G. Nyman, B. Petersen, M. Pfützner, A. Richter, K. Riisager, C. Scheidenberger, G. Schrieder, W. Schwab, H. Simon, M. H. Smedberg, M. Steiner, J. Stroth, A. Surowiec, T. Suzuki, O. Tengblad, M. V. Zhukov, Phys. Rev. **C59** (1999) 1152

[15] D. Aleksandrov, T. Aumann, L. Axelsson, T. Baumann, M.J.G. Borge, L. V. Chulkov, J. Cub, W. Dostal, B. Eberlein, Th. W. Elze, H. Emling, H. Geissel, V. Z. Goldberg, M. Golovkov, A. Grünschloß, M. Hellström, J. Holeczek, R. Holzmann, B. Jonson, A. A. Korsheninnikov, J. V. Kratz, G. Kraus, R. Kulessa, Y. Leifels, A. Leistenschneider, T. Leth, I. Mukha, G. Münzenberg, F. Nickel, T. Nilsson, G. Nyman, B. Petersen, M. Pfützner, A. Richter, K. Riisager, C.Scheidenberger, G. Schrieder, W. Schwab, H. Simon, M. H. Smedberg, M. Steiner, J. Stroth, A. Surowiec, T. Suzuki, O. Tengblad, M. V. Zhukov, Nucl. Phys. **A633** (1998) 234

[16] M. Zinser, F. Humbert, T. Nilsson, W. Schwab, T. Blaich, M.J.G. Borge, L.V. Chulkov, H. Eickhoff, T.W. Elze, H. Emling, B. Franzke, H. Freiesleben, H. Geissel, K. Grimm, D. Guillemaud-Mueller, P.G. Hansen, R. Holzmann, H. Irnich, B. Jonson, J.G. Keller, O. Klepper, H. Klingler, J.V. Kratz, R. Kulessa, D. Lambrecht, Y. Leifels, A. Magel, M. Mohar, A.C. Mueller, G. Münzenberg, F. Nickel, G. Nyman, A. Richter, K. Riisager, C. Scheidenberger, G. Schrieder, B.M. Sherrill, H. Simon, K. Stelzer, J. Stroth, O. Tengblad, W. Trautmann, E. Wajda, E. Zude, Phys. Rev. Lett. **75** (1995) 1719.

[17] D. Aleksandrov, T. Aumann, L. Axelsson, T. Baumann, M.J.G. Borge, L.V. Chulkov, J. Cub, W. Dostal, B. Eberlein, Th.W. Elze, H. Emling, H. Geissel, V.Z. Goldberg, M. Golovkov, A. Grünschloss, M. Hellström, J. Holeczek, R. Holzmann, B. Jonson, J.V. Kratz, G. Kraus, M. Meister, I. Mukha, G. Münzenberg, F. Nickel, T. Nilsson, G. Nyman, B. Petersen, M. Pfützner, V. Pribora, A. Richter, K. Riisager, C. Scheidenberger, G. Schrieder, W. Schwab, H. Simon, M.H. Smedberg, M. Steiner, J. Stroth, A. Suroviec, O. Tengblad, M.V. Zhukov, Nucl. Phys. **A669** (2000) 51

[18] Th. Blaich, Th. W. Elze, H. Emling, H. Freiesleben, K. Grimm, W. Henning, R. Holzmann, G. Ickert, J. G. Keller, H. Klingler, W. Kneissl, R. König, R. Kulessa, J. V. Kratz, D. Lambrecht, J. S. Lange, Y. Leifels, E. Lubkiewicz, M. Proft, W. Prokopowicz, C. Schütter, R. Schmidt, H. Spies, K. Stelzer, J. Stroth, W. Walus, E. Wajda, H. J. Wollersheim, M. Zinser, E. Zude, Nucl. Ins. and Meth. in Phys. Research **A314** (1992) 136

[19] M.V. Zhukov, B.V. Danilin, D.V. Fedorov, J.M. Bang, I.J. Thompson, J.S. Vaagen, Phys. Rep. **231** (1993) 151

[20] A.M. Lane, R.G. Thomas, Rev. Mod. Phys. **30** (1958) 257

[21] T.A. Tombrello, Phys. Rev. **143** (1966) 772

[22] T.W. Phillips, B.L. Berman, J.D. Seagrave, Phys. Rev. **C22** (1980) 384

[23] E.L. Berger, R. Singer, G.H. Thomas, T. Kafka, Phys. Rev. **D15** (1977) 206

[24] G. Jancso, M.G. Albrow, S. Almehed, P.S.L. Booth, X. De Bouard, J. Burger, H. Bøggild, L.J. Carroll, P. Catz, E. Dahl-Jensen, I. Dahl-Jensen, G. Damgaard, G. Von Dardel, N. Elverhaug, B. Guillerminet, K. Hansen, P. Herbsleb, J.N. Jackson, G. Jarlskog, H.B. Jensen, L. Jönsson, A. Klovning, E. Lillethun, R. Little, E. Lohse, A. Lu, B. Lörstad, N.A. Mccubbin, A. Melin, H.E. Miettinen, J.V. Morris, R. Møller, S. Ø. Nielsen, B.S. Nielsen, J.O. Petersen, T. Sanford, J.A.J. Skard, D.B. Smith, and P. Villeneuvex, Nucl. Phys. **B124** (1977) 1

[25] D. Drijard, H.G. Fischer, and T. Nakada, Nucl. Instr. and Meth. in Phys. Research, **225** (1984) 367

[26] J. Pochodzalla, C.K. Gelbke, W.G. Lynch, M. Maier, D. Ardouin, H. Delagrange, H. Doubre, C. Gregoire, A. Kyanowski, W. Mittig, A. Peghaire, J. Peter, F. Saint-Laurent, B. Zwieglinski, G. Bizard, F. Lefebvres, B. Tamain, J. Quebert, Y.P. Viyogi, W.A. Friedman, D.H. Boal, Phys. Rev. **C35** (1987) 1695

[27] L.M. Delves, Nucl. Phys. **20** (1960) 275

[28] B.V. Danilin, I.J. Thompson, J.S. Vaagen, M.V. Zhukov, Nucl. Phys. **A632** (1998) 383

[29] O.V. Bochkarev, L.V. Chulkov, A.A. Korsheninnikov, E.A. Kuzmin, I.G. Mukha, G.B. Yankov, Nucl. Phys. **A505** (1989) 215

[30] J. Raynal, J. Revai, Nuovo. Cim. **68A** (1970) 612

[31] N.K. Timofeyuk, Phys. Rev. **C65** (2002) 064306

[32] J.M. Bang, F.A. Gareev, G.S. Kazacha, A.M. Kalinin, Phys. Scr. **41** (1990) 202

[33] W.T. Eadie, D. Drijard, F.E. James, M. Roos, B. Sadoulet, Statistical Methods in Experimental Physics, North-Holland, (Amsterdam, 1971)

[34] CERN Program Library Long Writeup D506, MINUIT-Function Minimization and Error Analysis, Version 94.1, F. James, CERN, Geneva Switzerland, 1998